Vol 14 No 10, October 2005
1009-1963/2005/14(10)/2026-07

Chinese Physics

© 2005 Chin. Phys. Soc.
and IOP Publishing Ltd

Beam divergence effects on high power optical parametric oscillation

Li Hui-Qing(李惠青)[a)b)†], Geng Ai-Cong(耿爱丛)[a)b)], Bo Yong(薄 勇)[a)], Wu Ling-An(吴令安)[a)], Cui Da-Fu(崔大复)[a)], and Xu Zu-Yan(许祖彦)[a)]

[a)] *Beijing National Laboratory for Condensed Matter Physics, Institute of Physics, Chinese Academy of Sciences, Beijing* 100080, *China*

[b)] *Graduate School of the Chinese Academy of Sciences, Beijing* 100080, *China*

(Received 6 April 2005; revised manuscript received 26 May 2005)

The beam divergence effects of the input pump laser on a high power nanosecond optical parametric oscillator (OPO) have been numerically simulated. The OPO conversion efficiency is affected due to the angular deviation of real laser beams from ideal phase matching conditions. Our theoretical model is based on the decomposition of the Gaussian beam and assumes each component has a single deviation angle and thus a particular wave vector mismatch. We take into account the variable intensity profile in the spatial and temporal domains of the Gaussian beam, the pump depletion effects for large-signal processes as well as the oscillatory effects of the three waves. Two nonlinear crystals β-BaB_2O_4 (BBO) and LiB_3O_5 (LBO) have been investigated in detail. The results indicate that the degree of beam divergence strongly influences the maximum pump intensity, optimum crystal length and OPO conversion efficiency. The impact of beam divergence is much more severe in the case of critical phase-matching for BBO than in the case of non-critical phase-matching for LBO. The results provide a way to choose the optimum parameters for a high power ns OPO such as the nonlinear material, the crystal length and the pump intensity, etc. Good agreement is obtained with our experimental results.

Keywords: optical parametric oscillation, beam divergence effect, wave vector mismatch
PACC: 4265K, 4260K, 4265B

1. Introduction

Optical parametric oscillators (OPOs) pumped by intense laser pulses are powerful sources because of their coherence, broad tuning range, and high conversion efficiency.[1,2] Their wavelength tunability and high output power make them ideal light sources for an enormous number of applications, including light detection, free-space telecommunications, medical research, display technology, and welding. The development of high-power pump sources and high-quality nonlinear optical crystals with high damage threshold, such as β-BaB_2O_4 (BBO), LiB_3O_5 (LBO), $KTiOPO_4$ (KTP) and $KTiOAsO_4$ (KTA) promises even higher power and conversion efficiency OPOs.[3−5]

However, the pump laser beams from practical laser systems are not perfectly collimated and have a finite beam divergence. This means that some portions of the input beams will not be properly phase matched during the OPO processes, thus the conversion efficiency will be affected. When nanosecond (ns) pulses are used, longer interaction lengths in the crystals are required. Under these conditions, dephasing due to angular, spectral, and temperature bandwidths and crystal nonuniformity becomes important.

The simulations on ns OPO performance have been studied extensively by a number of authors.[6−12] Most analyses of these works were limited to small OPO conversion efficiencies with low pump depletion or beams without divergence. For examples, Brosnan and Byer[7] obtained an analytic expression to describe the parametric process based on nondiverging waves in the low depletion limit. Following this model Terry *et al*[8] added optical cavity modes but retained the assumption of low pump depletion. These models can predict only threshold characteristics but not the OPO conversion efficiency or power profile. Debuisschert[9] reported a semi-analytical model on ns OPOs which took into account the pump deple-

†E-mail: huiqing0910@yahoo.com

tion and the transverse profiles of the fields, but ignored the beam divergence. Similarly, Fix and Wallenstein [10] calculated the intensity of the output pulses, the total pulse energy, the efficiency, and the spectral distribution in the mode spectrum for OPO operation. Their model was based on numerical integration of the frequency-mixing equations by decomposition of the Gaussian pump pulse and included depletion effects. However, their analysis again neglected beam divergence. Very few papers have been published on ns OPO models that include both pump depletion and beam divergence. Arisholm[11] and Urschel *et al*[12] presented numerical models with pump depletion as well as the beam divergence. The former investigated the quantum noise initiation and macroscopic fluctuations in OPOs. The latter analysed the spatial behaviour of ns BBO-OPOs, and their calculations provided detailed information on the dependence of the OPO beam quality on pump energy. In this article we extend the calculation of Fix and Wallenstein and investigate theoretically the impact of a Gaussian pump beam's angular spectrum on ns OPO conversion efficiency in more detail, taking into account a variable intensity profile in the spatial and temporal domains of the Gaussian beam, birefringence, arbitrary cavity-mirror reflectivities, pump beam depletion effects for large-signal processes, as well as the round trips of the signal, idler and pump waves in the OPO cavity. The model is applied to critically phase-matched (CPM) BBO-OPO and non-critically phase-matched (NCPM) LBO-OPO. The results obtained in this paper suggest a way to choose the optimum parameters for a high-power ns OPO such as the nonlinear material, the crystal length and the pump intensity, etc.

2. Model formulation

OPO is a three-wave interaction process, in which pump, signal, and idler waves are involved. The coupled differential equations for their amplitudes are

$$\begin{cases} \dfrac{\mathrm{d}E_1}{\mathrm{d}z} + \alpha_1 E_1 = \mathrm{i}\kappa_1 E_3 E_2^* \mathrm{e}^{\mathrm{i}\Delta kz}, \\ \dfrac{\mathrm{d}E_2}{\mathrm{d}z} + \alpha_2 E_2 = \mathrm{i}\kappa_2 E_3 E_1^* \mathrm{e}^{\mathrm{i}\Delta kz}, \\ \dfrac{\mathrm{d}E_3}{\mathrm{d}z} + \alpha_3 E_3 = \mathrm{i}\kappa_3 E_2 E_1 \mathrm{e}^{-\mathrm{i}\Delta kz}, \end{cases} \tag{1}$$

where

$$\kappa_i = \frac{\omega_i}{n_i c} d_{\mathrm{eff}}, \quad i = 1, 2, 3, \tag{2}$$

and 1, 2 and 3 denote the signal, idler and pump waves, respectively. In Eq.(1), α_i is the loss coefficient of the OPO cavity and the nonlinear crystal, and $\Delta k = |\Delta \boldsymbol{k}|$ the wave vector mismatch. In Eq.(2), ω_i is the angular frequency, n_i the refractive index of the nonlinear crystal, and d_{eff} the effective nonlinear coefficient. The intensity I is given in terms of the electric field amplitude E by

$$I(r,t) = \frac{1}{2} nc\varepsilon_0 \left|E(r,t)\right|^2. \tag{3}$$

The amount of dephasing among the waves is described by the wave vector mismatch $\Delta \boldsymbol{k}$. In general, dephasing is due to the departure from the ideal phase matching condition in the parametric three-wave interaction:

$$\Delta \boldsymbol{k} = \boldsymbol{k}_p - \boldsymbol{k}_s - \boldsymbol{k}_i. \tag{4}$$

For a perfect Gaussian beam, the electric field amplitude distribution in the spatial and temporal domains can be written as

$$E(r,t) = E_0 \exp(-r^2(z)/w^2(z) \exp(-t^2/\tau^2), \tag{5}$$

where E_0 is the electric field amplitude in the centre of the beam, τ the laser pulse duration, and w the beam radius. The beam propagates according to the following equation:

$$w^2(z) = w_0^2 \left(1 + \left(M^2 \frac{\lambda (z - z_0)}{\pi w_0^2}\right)^2\right), \tag{6}$$

where w_0 is the beam waist radius, z is the longitudinal position (z_0 being the waist position), λ the wavelength and M^2 the beam quality factor. In this paper we consider a perfect Gaussian beam for which $M^2 = 1$. It is not difficult to generalize our model to the case with imperfect beam quality.

Any real laser beam consists of a superposition of waves with a distribution of divergence which contributes to dephasing in OPO. We represent the electric field for the incident pump as a sum of waves with many radial and temporal components:

$$A = \sum_{i=1}^{N} \sum_{j=1}^{M} A_0 \exp(-r_i^2(z)/w^2(z)) \exp(-t_j^2/\tau^2), \tag{7}$$

in which A is the real part of the electric field amplitude and A_0 is the value of A in the beam centre. The imaginary part has a similar expression. We divide the beam radius into N components and the pulse duration into M components. The components at different radial positions have different angular departures and thus give rise to different values of the wave vector mismatch Δk.

In a uniaxial crystal, type-I phase matching requires that the wave propagates in a direction making an angle θ with the optic axis (i.e., the crystallographic z axis) of the nonlinear crystal. Phase matching is achieved by selecting the correct angle $\theta = \theta_m$. If the wave vector direction of the three waves is $\Delta\theta$ away from θ_m (i.e., $\theta = \theta_m + \Delta\theta$), the mismatch Δk is given by

$$\Delta k = \frac{\omega_3}{c} n_3(\omega_3, \theta) - \frac{\omega_2}{c} n_2(\omega_2, \theta) - \frac{\omega_1}{c} n_1(\omega_1, \theta), \quad (8)$$

where n_i is the refractive index of the crystal for the ω_i wave, i=1, 2 or 3. By a Taylor expansion of Δk with respect to θ near $\theta = \theta_m$, we have

$$\Delta k = \Delta k|_{\theta=\theta_m} + \left.\frac{\mathrm{d}(\Delta k)}{\mathrm{d}\theta}\right|_{\theta=\theta_m} \Delta\theta + \frac{1}{2}\left.\frac{\mathrm{d}^2\Delta k}{\mathrm{d}\theta^2}\right|_{\theta=\theta_m} (\Delta\theta)^2 + \cdots. \quad (9)$$

For a negative uniaxial crystal such as BBO in type-I phase matching,

$$\begin{aligned} n_1(\omega_1, \theta) &= n_\mathrm{o}(\omega_1), \\ n_2(\omega_2, \theta) &= n_\mathrm{o}(\omega_2), \\ n_3(\omega_3, \theta) &= n_\mathrm{e}(\omega_3, \theta) \\ &= \left[\frac{n_\mathrm{o}^2(\omega_3)\, n_\mathrm{e}^2(\omega_3)}{n_\mathrm{o}^2(\omega_3)\sin^2\theta + n_\mathrm{e}^2(\omega_3)\cos^2\theta}\right]^{1/2}; \end{aligned} \quad (10)$$

thus

$$\begin{aligned} \frac{\mathrm{d}\Delta k}{\mathrm{d}\theta} &= \frac{\mathrm{d}K_3}{\mathrm{d}\theta} - \frac{\mathrm{d}K_2}{\mathrm{d}\theta} - \frac{\mathrm{d}K_1}{\mathrm{d}\theta} \\ &= \frac{\mathrm{d}K_3}{\mathrm{d}\theta} = \frac{\omega_3}{c}\frac{\mathrm{d}n_\mathrm{e}(\omega_3, \theta)}{\mathrm{d}\theta} \\ &= -\frac{1}{2}\frac{\omega_3}{c} n_\mathrm{e}^3(\omega_3, \theta) \\ &\quad \times \left[n_\mathrm{e}^{-2}(\omega_3) - n_\mathrm{o}^{-2}(\omega_3)\right]\sin 2\theta, \end{aligned} \quad (11)$$

$$\begin{aligned} \frac{\mathrm{d}^2\Delta k}{\mathrm{d}\theta^2} &= \frac{\mathrm{d}^2K_3}{\mathrm{d}\theta^2} = \frac{\omega_3}{c}\frac{\mathrm{d}^2 n_\mathrm{e}(\omega_3, \theta)}{\mathrm{d}\theta^2} \\ &= -\frac{1}{2}\frac{\omega_3}{c}\left[n_\mathrm{e}^{-2}(\omega_3) - n_\mathrm{o}^{-2}(\omega_3)\right] \\ &\quad \times \left[3n_\mathrm{e}^2(\omega_3, \theta)\frac{\mathrm{d}n_\mathrm{e}(\omega_3, \theta)}{\mathrm{d}\theta}\sin 2\theta \right. \\ &\quad \left. + 2n_\mathrm{e}^3(\omega_3, \theta)\cos 2\theta\right]. \end{aligned} \quad (12)$$

The Sellmeier equations for BBO can be written as[13]

$$\begin{aligned} n_\mathrm{o}^2 &= 2.7359 + \frac{0.01878}{\lambda^2 - 0.01822} - 0.01354\lambda^2, \\ n_\mathrm{e}^2 &= 2.3753 + \frac{0.01224}{\lambda^2 - 0.01667} - 0.01516\lambda^2, \end{aligned} \quad (13)$$

where λ is the wavelength in μm. By substituting Eq.(13) into Eq.(10) and using Eqs.(9)–(12), we can obtain the wave vector mismatch Δk for a type-I phase matched BBO crystal.

In a biaxial crystal, type-I phase matching requires that the wave propagates in the direction at an angle θ with the optic axis and an angle φ with the x-axis in the x-y plane of the nonlinear crystal, and the phase matching direction of the three waves is $(\theta_\mathrm{m}, \varphi_\mathrm{m})$. If the wave vector direction is $(\theta_\mathrm{m} + \Delta\theta,\ \varphi_\mathrm{m} + \Delta\varphi)$, we can also expand Δk into a Taylor series with respect to θ and φ near θ_m and φ_m, just as for a uniaxial crystal:

$$\Delta k = \Delta k|_{(\theta=\theta_\mathrm{m}, \varphi=\varphi_\mathrm{m})} + \left.\frac{\partial(\Delta k)}{\partial\theta}\right|_{(\theta=\theta_\mathrm{m}, \varphi=\varphi_\mathrm{m})} \Delta\theta + \frac{1}{2}\left.\frac{\partial^2\Delta k}{\partial\theta^2}\right|_{(\theta=\theta_\mathrm{m}, \varphi=\varphi_\mathrm{m})} (\Delta\theta)^2 + \cdots, \quad (14)$$

$$\Delta k = \Delta k|_{(\theta=\theta_\mathrm{m}, \varphi=\varphi_\mathrm{m})} + \left.\frac{\partial(\Delta k)}{\partial\varphi}\right|_{(\theta=\theta_\mathrm{m}, \varphi=\varphi_\mathrm{m})} \Delta\varphi + \frac{1}{2}\left.\frac{\partial^2\Delta k}{\partial\varphi^2}\right|_{(\theta=\theta_\mathrm{m}, \varphi=\varphi_\mathrm{m})} (\Delta\varphi)^2 + \cdots \quad (15)$$

From Eq.(8) we obtain

$$\frac{\partial\Delta k}{\partial\theta} = \frac{\omega_3}{c}\frac{\partial n(\omega_3)}{\partial\theta} - \frac{\omega_2}{c}\frac{\partial n(\omega_2)}{\partial\theta} - \frac{\omega_1}{c}\frac{\partial n(\omega_1)}{\partial\theta}, \quad (16)$$

$$\frac{\partial^2\Delta k}{\partial\theta^2} = \frac{\omega_3}{c}\frac{\partial^2 n(\omega_3)}{\partial\theta^2} - \frac{\omega_2}{c}\frac{\partial^2 n(\omega_2)}{\partial\theta^2} - \frac{\omega_1}{c}\frac{\partial^2 n(\omega_1)}{\partial\theta^2}, \quad (17)$$

$$\frac{\partial\Delta k}{\partial\varphi} = \frac{\omega_3}{c}\frac{\partial n(\omega_3)}{\partial\varphi} - \frac{\omega_2}{c}\frac{\partial n(\omega_2)}{\partial\varphi} - \frac{\omega_1}{c}\frac{\partial n(\omega_1)}{\partial\varphi}, \quad (18)$$

$$\frac{\partial^2\Delta k}{\partial\varphi^2} = \frac{\omega_3}{c}\frac{\partial^2 n(\omega_3)}{\partial\varphi^2} - \frac{\omega_2}{c}\frac{\partial^2 n(\omega_2)}{\partial\varphi^2} - \frac{\omega_1}{c}\frac{\partial^2 n(\omega_1)}{\partial\varphi^2}. \quad (19)$$

The refractive indices of the interaction waves along the wave vector direction (θ, φ) in a biaxial crystal can be expressed as

$$n(\omega_i) = \left(\frac{2}{-B_i \pm \sqrt{B_i^2 - 4C_i}}\right)^{1/2}, \quad (20)$$

where we take "–" when $i = 1, 2$ and "+" when $i = 3$ for type-I phase matching, and B_i and C_i are functions of θ and φ:

$$\begin{aligned} B_i &= -\sin^2\theta\cos^2\varphi\left[n_y^{-2}(\omega_i) + n_z^{-2}(\omega_i)\right] \\ &\quad - \sin^2\theta\sin^2\varphi\left[n_x^{-2}(\omega_i) + n_z^{-2}(\omega_i)\right] \\ &\quad - \cos^2\theta\left[n_x^{-2}(\omega_i) + n_y^{-2}(\omega_i)\right], \end{aligned} \quad (21)$$

$$\begin{aligned} C_i &= \sin^2\theta\cos^2\varphi n_y^{-2}(\omega_i)\, n_z^{-2}(\omega_i) \\ &\quad + \sin^2\theta\sin^2\varphi n_x^{-2}(\omega_i)\, n_z^{-2}(\omega_i) \\ &\quad + \cos^2\theta n_x^{-2}(\omega_i)\, n_y^{-2}(\omega_i). \end{aligned} \quad (22)$$

The derivatives of B_i and C_i with respect to θ and φ are

$$\begin{aligned}\frac{\partial B_i}{\partial\theta} =&[n_x^{-2}(\omega_i)+n_y^{-2}(\omega_i)-n_z^{-2}(\omega_i)\\ &-n_x^{-2}(\omega_i)\sin^2\varphi\\ &-n_y^{-2}(\omega_i)\cos^2\varphi]\sin 2\theta, \qquad (23)\\ \frac{\partial C_i}{\partial\theta} =&[n_y^{-2}(\omega_i)n_z^{-2}(\omega_i)\cos^2\varphi\\ &+n_x^{-2}(\omega_i)n_z^{-2}(\omega_i)\sin^2\varphi\\ &-n_x^{-2}(\omega_i)n_y^{-2}(\omega_i)]\sin 2\theta, \qquad (24)\\ \frac{\partial B_i}{\partial\varphi} =&\left[n_y^{-2}(\omega_i)-n_x^{-2}(\omega_i)\right]\sin^2\theta\sin 2\varphi, \qquad (25)\\ \frac{\partial C_i}{\partial\varphi} =&\left[n_x^{-2}(\omega_i)-n_y^{-2}(\omega_i)\right]n_z^{-2}(\omega_i)\sin^2\theta\sin 2\varphi. \qquad (26)\end{aligned}$$

The derivatives of Eq.(20) can be expressed as

$$\begin{aligned}\frac{\partial n(\omega_i)}{\partial\theta} =&-\frac{\sqrt{2}}{2}\left(-B_i\pm\sqrt{B_i^2-4C_i}\right)^{-3/2}\\ &\times\left(-\frac{\partial B_i}{\partial\theta}\pm\frac{B_i\dfrac{\partial B_i}{\partial\theta}-2\dfrac{\partial C_i}{\partial\theta}}{\sqrt{B_i^2-4C_i}}\right), \qquad (27)\\ \frac{\partial^2 n(\omega_i)}{\partial\theta^2} =&\frac{\partial}{\partial\theta}\left[\frac{\partial n(\omega_i)}{\partial\theta}\right], \qquad (28)\\ \frac{\partial n(\omega_i)}{\partial\varphi} =&-\frac{\sqrt{2}}{2}\left(-B_i\pm\sqrt{B_i^2-4C_i}\right)^{-3/2}\\ &\times\left(-\frac{\partial B_i}{\partial\varphi}\pm\frac{B_i\dfrac{\partial B_i}{\partial\varphi}-2\dfrac{\partial C_i}{\partial\varphi}}{\sqrt{B_i^2-4C_i}}\right), \qquad (29)\\ \frac{\partial^2 n(\omega_i)}{\partial\varphi^2} =&\frac{\partial}{\partial\varphi}\left[\frac{\partial n(\omega_i)}{\partial\varphi}\right]. \qquad (30)\end{aligned}$$

For LBO, the Sellmeier equations are[14]

$$\begin{aligned}n_x^2 =&2.4542+\frac{0.01125}{\lambda^2-0.01135}-0.01388\lambda^2,\\ n_y^2 =&2.5390+\frac{0.01277}{\lambda^2-0.01189}-0.01849\lambda^2\\ &+4.3025\times10^{-5}\lambda^4-2.9131\times10^{-5}\lambda^6,\\ n_z^2 =&2.5865+\frac{0.01310}{\lambda^2-0.01223}-0.01862\lambda^2\\ &+4.5778\times10^{-5}\lambda^4-3.2526\times10^{-5}\lambda^6. \qquad (31)\end{aligned}$$

Substituting Eq.(31) into Eqs.(21)–(26) and then substituting Eqs.(21)–(26) into Eq.(27)–(30), we can obtain the wave vector mismatch Δk for type-I phase matched LBO from Eqs.(14)–(19).

For a high conversion efficiency OPO, no analytical solution is possible. We solve the coupled OPO differential equations (1) numerically using a fourth-order Runge–Kutta integration routine. The required number of integration times and beam radius components are determined by checking the resulting convergence. The number of pulse duration components is determined by the number of round trips of the pump pulse in the OPO cavity. In our computational procedure we introduce a variable beam intensity along the propagation direction of the three waves due to the propagation characteristics of a Gaussian beam. Differing from an OPA, for the OPO we take into account the oscillatory effect of the three waves by considering the reflection coefficients of the two OPO cavity mirrors for the pump, signal and idler waves.

3. Computational results and discussion

We now proceed to calculate the influence of the angular divergence in an actual high-power OPO. In our simulation, the OPO pump source is a 532 nm green laser with a pulse duration of 50 ns and repetition rate of 10 kHz. The OPO process used is 532 nm (e)=900 nm (o)+1301 (o) and the signal wavelength is 900 nm. We consider the single idler-resonant OPO in which only the signal wave is output. The input cavity mirror of the OPO has a partial transmission of 65% for the pump laser. It is highly reflective for the signal and idler waves, with reflectivities of 99.9% and 99.8%, respectively. The output cavity mirror is anti-reflective for the signal (transmission 94.5%) and highly reflective for the pump and idler waves (reflectivity 99.7% and 99.8%, respectively). In this case we have to take into account the back reflection of the pump and oscillation of the idler beam. In the following calculations, two different crystals, BBO and LBO, are considered. The BBO-OPO is in the CPM configuration and the LBO-OPO is in the NCPM configuration which can be achieved by heating the LBO crystal. In our calculation, we do not consider the walk-off effect for the case of CPM BBO-OPO in which walk-off exists. The essential processes of the interactions of the Gaussian beams allow us to characterize the effects of the beam divergence on the conversion efficiency. For NCPM LBO-OPO, there is no walk-off effect.

Figures 1(a) and (b) show the signal conversion efficiency as a function of interaction length at a pump intensity of 90MW/cm^2 for several divergence angles in BBO and LBO, respectively. There are a number of observations to be noted. The OPO signal conversion efficiency is larger for a smaller beam divergence. There is an optimum length of the crystal to maximize

the OPO signal conversion for a given pump intensity and beam divergence. Due to the back-conversion from the signal and idler waves to the pump wave in the case of high efficiency and long crystal length, an oscillating structure appears in the OPO conversion along the length of the crystal. With the increase of the beam divergence, the maximum signal conversion shifts to a shorter crystal length. We note the same qualitative behaviour for both CPM BBO-OPO and NCPM LBO-OPO, but LBO exhibits one order of magnitude greater divergence tolerance than BBO. For the same divergence angle, a longer optimum crystal length and hence higher conversion efficiency can be obtained by using LBO instead of BBO crystal.

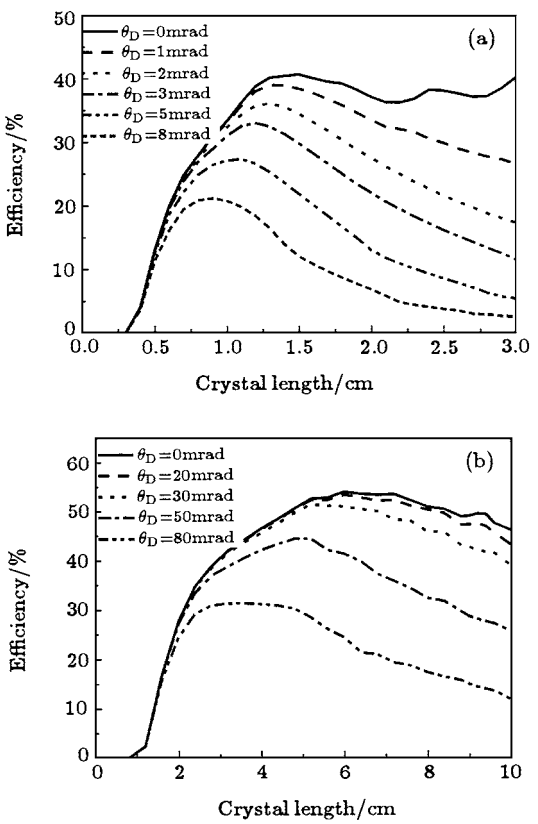


Fig.1. Signal efficiency versus crystal length for different divergence angles for: (a) BBO and (b) LBO. Simulation parameters: pump intensity I_p=90MW/cm^2.

The computed signal conversion efficiency as a function of pump intensity for different values of beam divergence is illustrated in Figs.2(a) and (b). For a given crystal length, the signal conversion efficiency decreases with increasing beam divergence for both BBO and LBO. However, the conversion efficiency drops more slowly for LBO than for BBO. Also, for higher pump intensities (usually corresponding to higher pump power) the conversion efficiency with LBO is higher than with BBO, so higher OPO output power can be achieved with LBO.

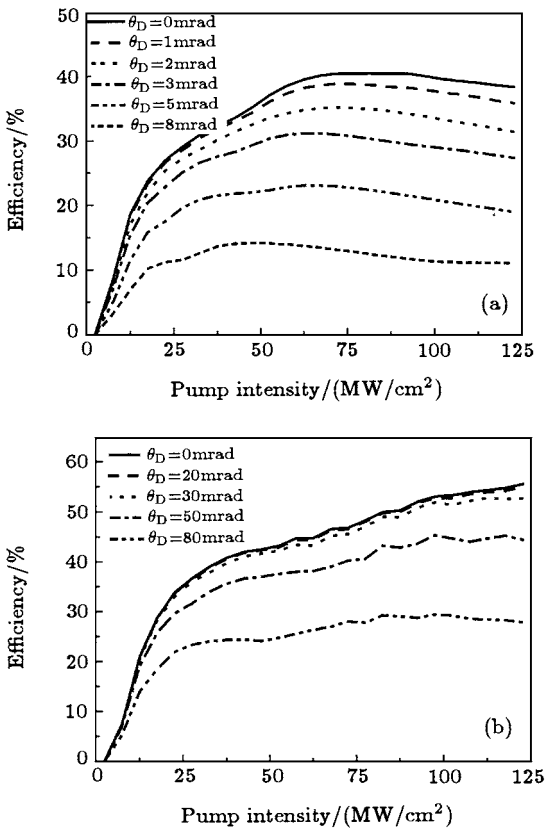


Fig.2. Signal efficiency versus pump intensity for different divergence angles for: (a) BBO, crystal length=1.5cm and (b) LBO, crystal length=5.0cm.

The OPO signal conversion efficiency can also be examined as a function of the laser input intensity for different crystal lengths at a given beam divergence. Figures 3(a) and (b) show the conversion efficiency for various crystal lengths for BBO at θ_D=1.0mrad and LBO at θ_D=30mrad, respectively. Similarly, Figs.4(a) and (b) show the conversion efficiency for BBO at θ_D=5.0mrad and LBO at θ_D=80mrad, respectively. It can be seen again from Figs.3(a), 3(b), 4(a) and (b) that the optimum crystal length tends to be shorter and the maximum conversion efficiency lower when the beam divergence angle increases.

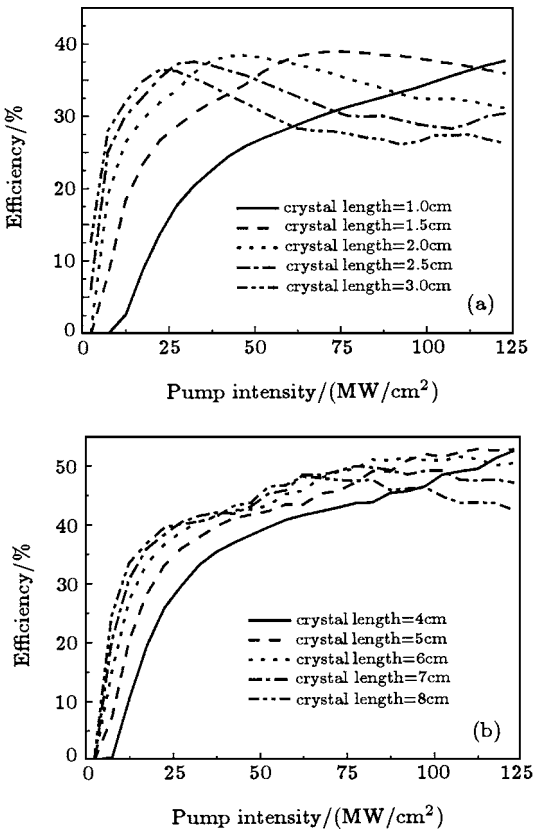


Fig.3. Signal efficiency versus pump intensity for different crystal lengths for: (a) BBO, θ_D=1.0mrad and (b) LBO, θ_D=30mrad.

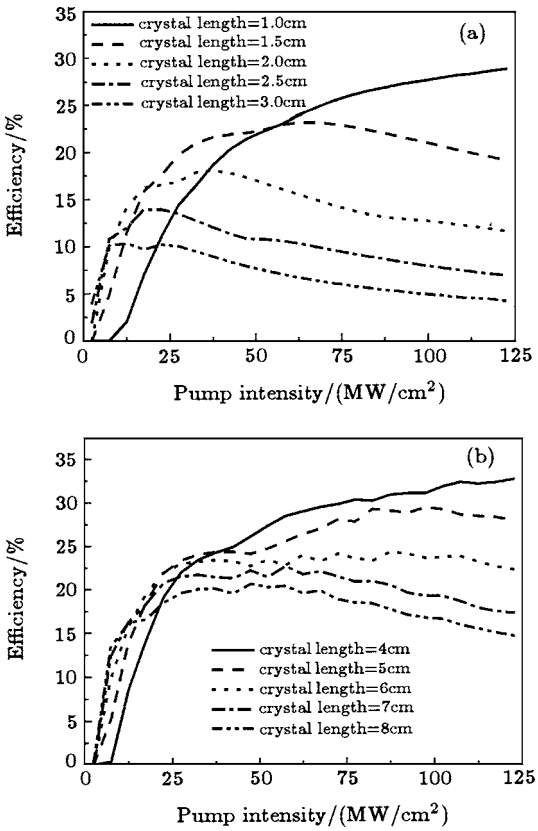


Fig.4. Signal efficiency versus pump intensity for different crystal lengths for: (a) BBO, θ_D=5.0mrad and (b) LBO, θ_D=80mrad.

To summarize the above results, the beam divergence in a nonlinear crystal decreases the OPO efficiency. Since LBO exhibits greater divergence tolerance than BBO, a longer optimum crystal length and higher conversion efficiency can be obtained by using LBO in a high-power ns OPO.

Our model has been compared with the experimental results of our OPO,[4] where a 50 mm long NCPM LBO crystal was employed. The 532 nm green pump laser (50ns, 10kHz) was a focused beam of divergence angle 12.5mrad, which corresponds to the case of θ_D=0mrad to θ_D=20mrad in Fig.1(b). The input and output mirror parameters were the same as those in our simulation. Through optimization of the design parameters, up to 13.5W of average signal power was obtained with a conversion efficiency of 50% for a pump intensity of 135MW/cm^2. These experimental results are in good agreement with our numerical simulation.

4. Conclusion

A numerical model has been developed to simulate the beam divergence effects on a high-power ns OPO. Our model is based on a decomposition of the Gaussian beam, with different components having different deviation angles and thus different wave vector mismatch values. We have taken into account the birefringence, variable intensity profile in the spatial and temporal domains, and the oscillation of the three waves in the OPO cavity.

The effects of beam divergence on conversion efficiency have been analysed for two nonlinear crystals BBO and LBO in the cases of critical and non-critical phase-matching, respectively. The computed results indicate that the degree of beam divergence has a strong influence on the maximum pump intensity, optimum crystal length and OPO conversion efficiency. The impact of beam divergence is much more severe in the case of BBO-OPO than in the case of LBO-OPO.

The results obtained in this paper can help us choose the optimum parameters for the nonlinear material, crystal length, pump intensity etc when designing a high-power ns OPO. Besides the OPO conversion efficiency, using our model we can also numerically

simulate the OPO output energy (power), the intensities of the signal, idler and depleted pump beams, the temporal pulse profile, as well as the beam's spatial distribution.

References

[1] Byer R L and Herbst R L 1977 *Top. Appl. Phys., Nonlin. Infrared Gen.* **16** 81

[2] Lin X C, Kong Y P, Zhang Y, Zhang J, Yao A Y, Bi Y, Sun Z P, Cui D F, Li R N, Wu L A and Xu Z Y 2004 *Chin. Phys.* **13** 1042

[3] Webb M S, Moulton P F, Kasinski J J, Burnham R L, Loiacono G and Stolzenberger R 1998 *Opt. Lett.* **23** 1161

[4] Li H Q, Zhang H B, Bao Z, Zhang J, Sun Z P, Kong Y P, Bi Y, Lin X C, Yao A Y, Wang G L, Hou W, Li R N, Cui D F and Xu Z Y 2004 *Opt. Commun.* **232** 411

[5] Liu H J, Chen G F, Zhao W, Wang Y S and Zhao S H 2001 *Acta Phys. Sin.* **50** 1717 (in Chinese)

[6] Bjorkholm J E 1971 *IEEE J.Q.E.* **QE-7** 109

[7] Brosnan S J and Byer R L 1979 *IEEE J.Q.E.* **QE-15** 415

[8] Terry J A C, Cui Y, Yang Y, Sibbett W and Dunn M H 1994 *J. Opt. Soc. Am.* B **11** 758

[9] Debuisschert T 1997 *Quantum Semiclass. Opt. J. Appl. Phys.* **9** 209

[10] Fix A and Wallenstein R 1996 *J. Opt. Soc. Am.* B **13** 2484

[11] Arisholm G 1999 *J. Opt. Soc. Am.* B **16** 117

[12] Urschel R, Borsutzky A and Wallenstein R 2000 *Appl. Phys.* B **70** 203

[13] Kato K 1986*IEEE J. Quantum Electron* **QE-22** 1013

[14] Kato K 1994 *IEEE J. Quantum Electron* **30** 2950